Multi-wavelength photo-acoustic microscopy in the frequency domain for simultaneous excitation and detection of dyes

Olivier Hugon, Boudewijn van Der Sanden, Mehdi Inglebert, Olivier Jacquin, Chaouqi Misbah, Eric Lacot

Research Article | Vol. 10, No. 2 | 1 Feb 2019 | BIOMEDICAL OPTICS EXPRESS 932
Biomedical Optics EXPRESS

Multi-wavelength photo-acoustic microscopy in the frequency domain for simultaneous excitation and detection of dyes

OLIVIER HUGON,[1,*] BOUDEWIJN VAN DER SANDEN,[2] MEHDI INGLEBERT,[1] OLIVIER JACQUIN,[1] CHAOUQI MISBAH,[1] AND ERIC LACOT[1]

[1]*Univ. Grenoble Alpes, CNRS, LiPhy, F-38000 Grenoble, France*
[2]*Univ. Grenoble Alpes, CNRS, TIMC-IMAG UMR 5525, La Tronche, France*
**olivier.hugon@univ-grenoble-alpes.fr*

Abstract: An optical-resolution photoacoustic microscope with modulated CW laser diodes allowing multi-channel imaging is presented that can be used for both imaging biological tissues and for targeted photo-dynamic therapy (PDT) varying the optical power and exposure time. The effects of this therapy are immediately monitored in order to optimize the time of irradiation. After the description of the experimental setup, *in vitro* and *in vivo* applications are presented on a synthetic sample and on the mouse ear using hemoglobin as endogenous and methylene blue as exogenous dye for imaging and PDT, respectively.

1. Introduction

In clinic, there is an important need for handheld imaging equipment for the detection of microscopic effects of anti-cancer therapies. These have multiple effects on tissue parameters, concerning tumor (micro)-vessels, different cell types, and inflammation processes. These effects are either anti- or pro-tumoral and often stimulate recurrence in time [1]. Until now, there are no clinical data available on these processes, because low cost imaging techniques for frequently monitoring in a personalized treatment planning and follow-up are absent. Most conventional medical imaging techniques are expensive, unable to resolve tissues at the microscopic level.

Recent clinical studies have shown that microscopic details of the tumor vessels in human breast cancer can be screened by photo-acoustic (PA) imaging to a depth of a few centimeters [2]. The technique may use endogenous dyes e.g. hemoglobin (Hb) or exogenous clinical dyes. PA-imaging has the potential to be low cost, and handheld for *in vivo* imaging with either a microscopic optical resolution or with a mesoscopic acoustic resolution.

In this preclinical proof of principle study, we focus on optical-resolution photoacoustic microscopy (OR-PAM) using modulated CW laser diodes. This allows simultaneous multi-channel imaging with a simple device without a high bandwidth or temporal multiplexing in comparison to time domain (TD) systems [3,4]. In comparison to TD excitation, the generation of acoustic pressure waves is usually less effective for frequency domain (FD) excitation. However, narrowband signal detection may be very effective, especially by the use of a matched filter or a resonant detector. A recent study has shown that the signal-to-noise ratio in FD photo-acoustics can be equal to or even higher than that of TD photo-acoustics under certain conditions [5]. Furthermore, CW laser diodes are more cost effective, come with smaller footprints and require less maintenance compared to the Q-switched ns-lasers typically used in TD systems. After a short description and validation of our setup, we will demonstrate that simultaneous excitation and detection of multiple dyes is possible in monitoring acute effects of a photo-dynamic therapy.

In photo-dynamic therapy (PDT), photosensitizing agents are used for selectively killing cancer cells or tumor blood vessels after local exposure to light photons [6]. This therapy is

#347565 https://doi.org/10.1364/BOE.10.000932
Journal © 2019 Received 9 Oct 2018; revised 28 Nov 2018; accepted 9 Dec 2018; published 29 Jan 2019

Biomedical Optics EXPRESS

tested in clinical trials for the treatment of residual tumor cells after resection [7]. Recently, the clinical dye methylene blue (MB) has been successfully used for PDT in preclinical studies [8–10]. Here, we demonstrated that photo-activation of MB in micro-vessels and simultaneous monitoring of the red blood cell distribution is possible on the PA-microscope. Different groups have proven the feasibility of PA microscopy and imaging *in vivo*, but only few [11] focused on low cost equipment with the use of different laser diodes for the simultaneous excitation of several endogenous and exogenous PA dyes.

The aim is to proof the principle that photo-dynamic therapy and *in vivo* monitoring of the effects on the microvasculature can be performed simultaneously when the intensities of CW laser diodes are frequency encoded on a photo-acoustic microscope.

2. Material and methods

2.1 Experimental setup

The experimental setup is described in Fig. 1. The collimated beams of two CW laser diodes (Omicron PhoxX laser diodes @ λ_1 = 415 nm and λ_2 = 660 nm) are combined with a dichroic mirror (Omicron LightHub). The laser diodes intensities are sinus modulated at f_1 = 5 MHz and f_2 = 5.3 MHz respectively, which ensures good channel isolation (see detection bandwidth below). The modulation signals are provided by a dual channel function generator (Tektronics, AFG3102C). Both beams have the same waist ω_0 = 350 µm and the same quality factor M^2 = 1.06 at the output of the laser diodes. The width of the beams is then increased by a factor of 10 by means of an afocal system in order to match the diameter of the entrance pupil of the microscope objective (Zeiss LD Epiplan 20X/0.4). This is the best compromise between resolution and loss of power. The resolution is of the order of 1 µm at 415 nm and 1.6 µm at 660 nm. The mean optical powers on the target are set between 2 mW and 6 mW for the two wavelength. A two-axis galvanometric mirror scanner makes it possible to move the beams on the surface of the target to build an image, with a pixel dwell time of 150 µs. The position of the target is set by a motorized three-axis translation stage. The PA signal is collected through an ultrasound transmission chamber by a focused piezoelectric transducer (NDT Systems, IBMF054) in a confocal arrangement. The acoustic probe has a focal distance of 1”, which is large enough that heating of the transducer by direct laser irradiation can be neglected. The transmission chamber is filled with a mixture of 50% ultrasonic gel (modul diagram, UG0260A2) and deionized water to achieve a compromise between ease of handling and acoustic impedance matching with the transducer. The electric signal from the acoustic probe is finally amplified (R&K, LA110-0S) and demodulated by two lock-in amplifiers (Stanford Research Systems, SR844), respectively running at f_1 and f_2 in a bandwidth of 3.2 kHz, to recover both the amplitudes of the PA signals generated at λ_1 and λ_2.

Biomedical Optics EXPRESS

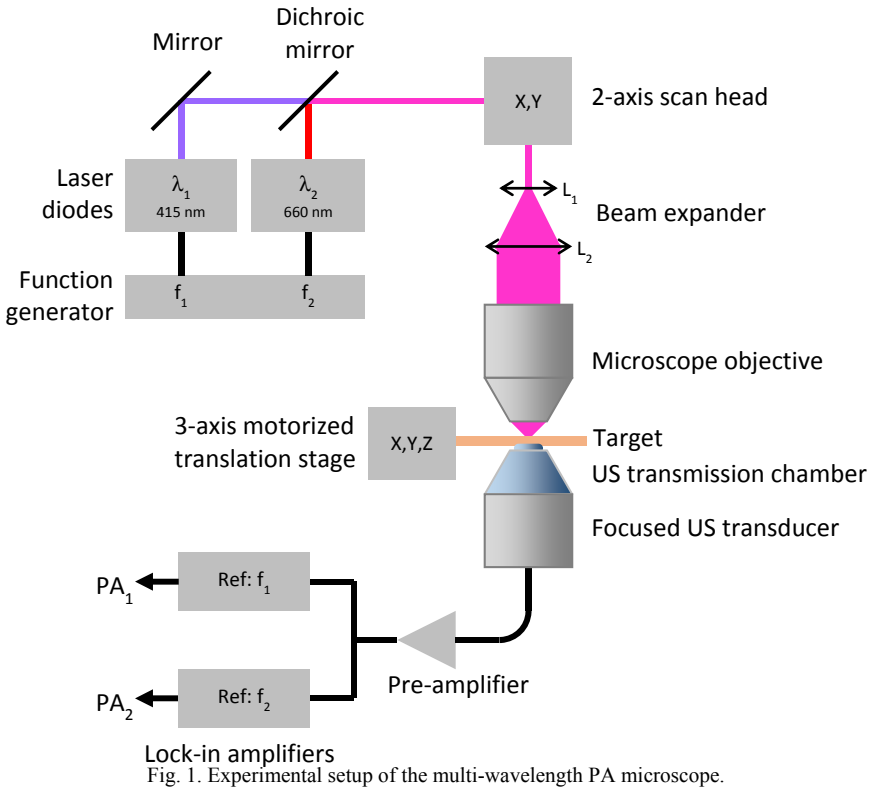

Fig. 1. Experimental setup of the multi-wavelength PA microscope.

2.2 Animal model

PA experiments were performed on the ears of white CD-1 IGS mice (Charles River, Écully, France). All efforts were made to minimize their number. They were housed in ventilated cages with food and water *ad libitum* in a 12 h light/dark cycle at 22 ± 1°C. For the experience, mice were anesthetized by an intraperitonial injection of ketamine (0.1 mg/g, Imalgene 1000, Boehringer Ingelheim) / xylazine (0.01 mg/g, ROMPUN Bayer) mixture. Their body temperature was maintained at 36 – 37° C using an electric heating pad with a feedback system. In experiments with dye infusion, mice were cannulated in a caudal vein (BD NeoflonTM, 16GA 0.6 x 19mm, Becton Dickinson, Helsingborg Sweden) and connected to a 1 ml syringe on an infusion pump with a target volume of 0.2 ml/min. In photo-dynamic therapy experiments, the concentration of the infused methylene blue solution was 0.2 mg/ml (M9140-100g, SIGMA Alderich France). Before positioning the ear on the lid of a petri dish (Ø = 10mm) in the focal plane of the objective with ultrasound gel, ears were cleaned with a hear-removing cream (VEET, France) and rinsed with 70% ethanol.

In accordance with the policy of Clinatec (permit number: B38-185 10 003) and the French legislation, experiments were done in compliance with the European Parliament and the Council Directive of September 22, 2010 (2010/63/EU). The research involving animals was authorized by the Direction Départementale des Services Vétérinaires de l'Isère – Ministère de l'Agriculture et de la Pêche, and the Ministère de l'Enseignement Supérieur et de la Recherche, France permit number: 2015051914157522_v1 (PI: B. van der Sanden, permit number 38 09 40 for animal experiences).

Biomedical Optics EXPRESS

2.3 Image processing and analysis

All PA images were processed and analyzed using Image-J software: version ImageJ 1.51 u, Wayne Rasband, NIH, USA, http://imagej.nih.gov/ij, Java 1.8.0_66 (64 bit). Composite images are used to highlight changes in the hematocrit distribution in the whole vessel network. The LUT of the sum of reference Hb PA images before a change is set to red and the LUT of the sum of Hb PA images after a change is set to green. The number of images for the calculation of the sum before and after a change is equal. In this case, a composite image indicates an increase of hematocrit in green and a decrease is coded red. Vessels are coded yellow (= red + green) when no change in hematocrit occurs and become orange for transient modulations of the Hb PA signal. This is perfectly illustrated in Fig. 6(d) and 6(e). Most PA images in Figs. 4, 6 and 7 had a background correction using a rolling ball algorithm with a radius of 20 pixels.

All graphs in the paper, statistics and linear regression analysis were generated by GraphPad PRISM version 3.02, 2000 (Graphpad Software, Inc). In Figs. 4, 5 & 6, signal to noise ratios of Hb PA signals in vessels were obtained after dividing the PA signal amplitudes by the mean signal amplitude of the background. For all regions of interest (ROI), signal to noise ratio analyses in time were performed with similar areas.

3. Results

The first section describes an in vitro validation of the multi-wavelength PA microscope followed by a proof of principle *in vivo* PDT study on the mouse ear.

3.1 In vitro validation of the PA microscope

Nowadays, there are no regular test samples to measure and validate signal to noise ratios of the PA signals as a function of the dye concentration for different excitation wavelengths. Therefore, we present here a simple and reproducible test sample in Fig. 2(a) and 2(d), which contains the primary colors of a laser printer: yellow, cyan and magenta. The surface concentration of the dyes (number of printed dots per unit area) was varied using different transparencies of a colored pattern, printed on a transparency for overhead projector (see Fig. 2(a)). The normalized concentration is determined by taking the highest concentration as the reference. A normalized concentration of 100% corresponds to a transparency of 0% and vice-versa. The PA signal amplitudes were linearly related to the dye concentration as depicted in Fig. 2(c). Similar results were obtained for cyan (λ_2 = 660 nm), but not shown.

Biomedical Optics EXPRESS

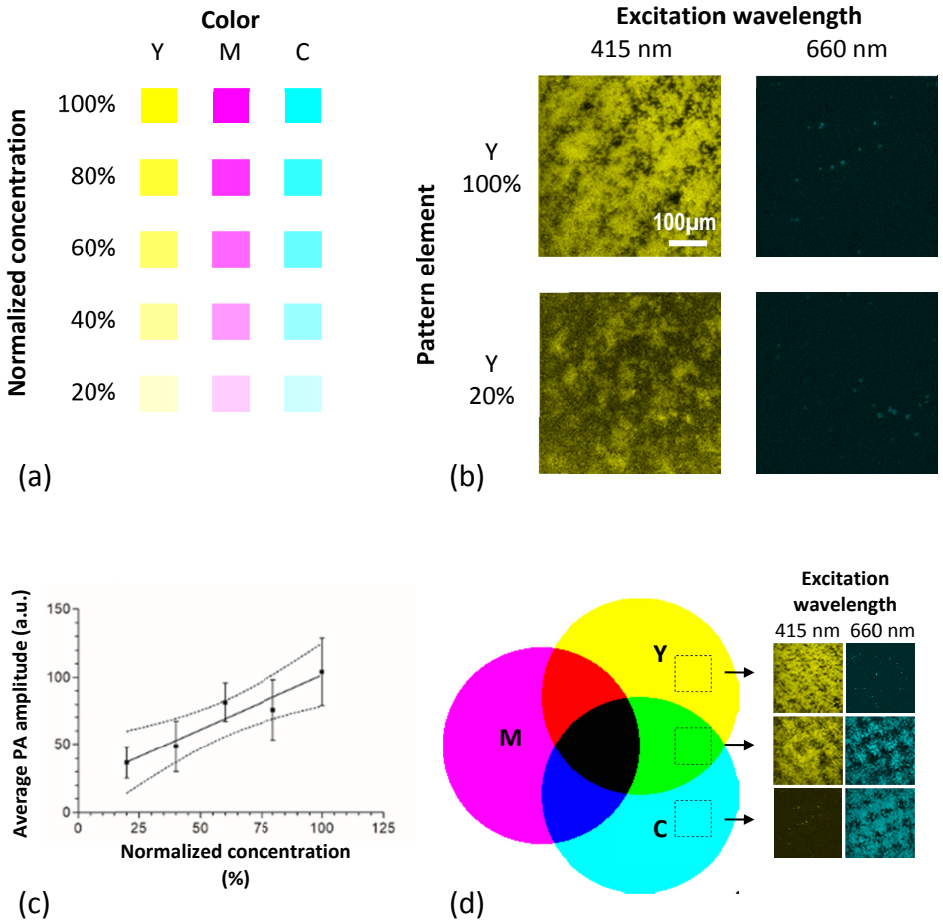

Fig. 2. Description and utilization of a synthetic test sample for the validation of the multi-wavelength PA microscope. (a) Pattern for testing the PA signal as a function of the dyes surface concentration. (b) PA images of the yellow dye at 100% and 20% concentrations with the excitation wavelength λ_1 = 415 nm and λ_2 = 660 nm. (c) Surface average of the PA amplitude ± the standard deviation for all concentrations. Results of the linear regression are depicted (R^2 = 0.91) with 95% confidence intervals (dotted line). (d) Pattern for testing the PA signal specificity with a dye mix. On the PA images on the right side, there is no visible response for the yellow dye at 660 nm and for the cyan dye at 415 nm. One can see that the images of the green area (yellow and cyan dyes mix) are complementary.

The absorption spectra of the yellow and cyan dyes have been measured (see Fig. 3(a)). The yellow dye has little or no absorption at the maximum absorption peak of cyan. However, at the maximum absorption of the yellow dye, little absorption of cyan is present. This gives no visible cross talking with the current sensitivity of the piezoelectric transducer during the simultaneous excitation and detection of the yellow and cyan dyes (see Fig. 2(b) & 2(d)). These dyes were chosen on purpose to prepare the *in vivo* experiences on the mouse ear: maximum absorption of HbO_2 is at λ_1 = 415 nm, and at λ_2 = 660 nm for MB (see absorption spectra in Fig. 3(b)).

Finally, it can be seen that the difference between the focusing planes at the two wavelengths is less than the field depth because the images of the two channels are both sharp in the green area of Fig. 2(d).

Biomedical Optics EXPRESS

In summary, real simultaneous excitation and detection of different PA dyes is possible and the surface average PA-signal amplitudes are linearly related to the surface concentration of the dyes at constant laser irradiance and dye temperature.

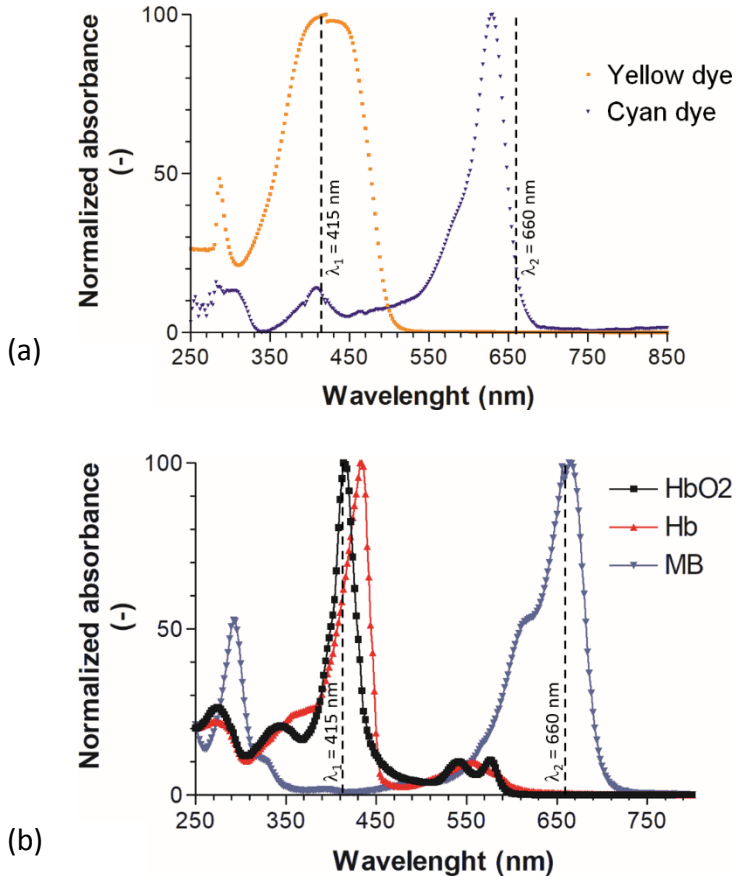

Fig. 3. (a) Normalized absorption spectra of the yellow and the cyan dyes. At $\lambda_1 = 415$ nm, the absorption of the yellow dye is close to its maximum, the cyan dye has a small absorption peak but hardly detectable with the current photo-acoustic sensitivity of the piezo-electric transducer. At $\lambda_2 = 660$ nm, there is no absorption of the yellow dye. (b) Normalized absorption spectra of HbO_2, Hb and MB. The maximum absorption of HbO_2 is at 415 nm and at 660 nm for methylene blue (MB) (see website of the Oregon Medical Laser Center in Portland https://omlc.org/spectra/index.html).

3.2 Photo-acoustic microscopy and photo-dynamic therapy

The current PA microscope can be used simultaneously for PA imaging and PDT. In our setup, the same laser diodes are used for both applications. In the imaging mode, an overview image may indicate the ROIs for PDT using single point excitations. Before combining PA microscopic imaging and PDT, it is important to analyze possible tissue laser damage during imaging at the absence of photo sensitive dyes. In the imaging mode, the maximum 415nm laser diode power is set to 2.3 mW at the entrance of the skin and the dwell time is 150 µs. The average speed of red blood cells (RBC) in the capillaries is 130 µm/s [12]. During the pixel dwell time, the RBCs have moved 0.02 µm, which is small compared with their size (6-8 µm). One can then assume that the RBCs are stationary during a pixel acquisition. Therefore, the average of the PA amplitude in a capillary is proportional to the hematocrit. On

Biomedical Optics EXPRESS

the composite image in Fig. 4(c), yellow coded vessels indicate no change in RBC distribution. We can see that there is no tissue damage within 10 minutes in the imaging mode, although we are a priori above the American National Standards Institute (ANSI) laser safety limit (0.8 kW/cm^2 for an exposition time of 150 µs) if we consider the irradiance at the optical focus in air (150 kW/cm^2). Actually, this safety limit needs clarification for the present problem. Indeed, the laser beam is focused under the surface of the skin. First, the radius of the exposed area on the surface of the skin is much larger than the beam waist because of convergence. On this basis, our estimate shows that the irradiance at the surface is below the safety limit. Then, some of the light is reflected by the surface of the skin (up to 30%, depending on the skin color). The rest undergoes scattering through the tissue before reaching the focal plane, where only a fraction of the initial light is concentrated. Finally, the local heat in the functional vessels is rapidly dispatched in comparison to the therapy mode with higher incident power and exposure time.

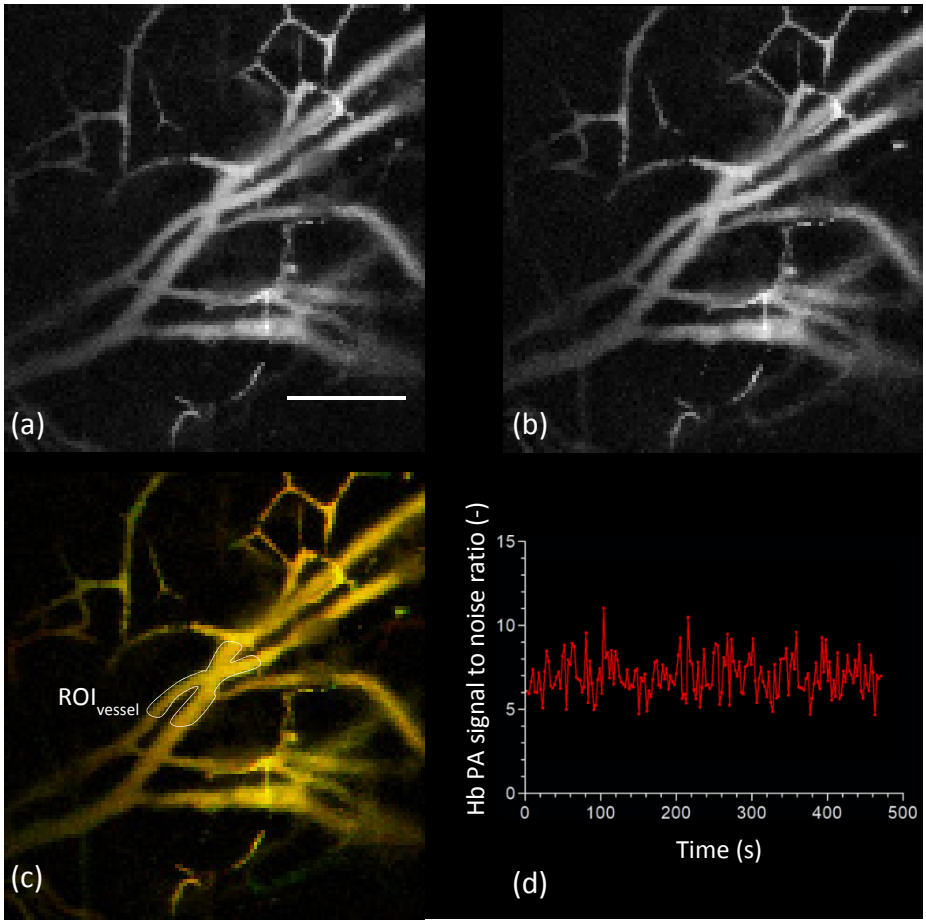

Fig. 4. Control of possible laser damage on the microvasculature in mouse ear for the imaging mode. The diode laser at 415 nm was set to 2.3 mW. The scale bar in (a) = 50 µm. (a) The sum of the first 25 images in the time series after background correction (rolling ball radius = 20 pixels). (b) The sum of 25 images (125-150) near the end of the time series with background correction, see (a). (c) Composite image of (a) in red and (b) in green showing most vessels in yellow (= red + green), which means no change in RBC distribution. (d) Graph of the Hb PA signal to noise ratios in time for the depicted vessel (see region of interest ROI$_{vessel}$).

In this paragraph, we analyzed the effect of a 1 minute single point laser irradiation for the 415 nm laser diode at 2.3, 3.6 and 6.1 mW (therapy mode). The effect on blood clotting was

Biomedical Optics EXPRESS

immediate in the region of interest (ROI) covering the location of the laser heating; see Fig. 5(d) and red signals in 5a-5c at a depth of maximum 100 µm beneath the skin. The degree of clotting was laser power dependent, see Fig. 5(d). In the composite images 5a-5c, the red PA signals are the sum of all slices in a time series before irradiation and the green signal equals the sum of all slices after irradiation. When red signals dominate (see dotted circles), the vessel obstruction was nearly complete with little or no RBC flux (Hb PA signals). Only the highest laser power resulted in a nearly complete vessel obstruction, see green curve in (d) in comparison to the background PA signal to noise ratios (white curve).

In summary, the imaging mode had no effect on the RBC distribution and vessel morphology in comparison to the therapy mode with a longer duration single point laser excitation. Previous characterization of the PA-microscope allowed further *in vivo* studies as reported in the next paragraph.

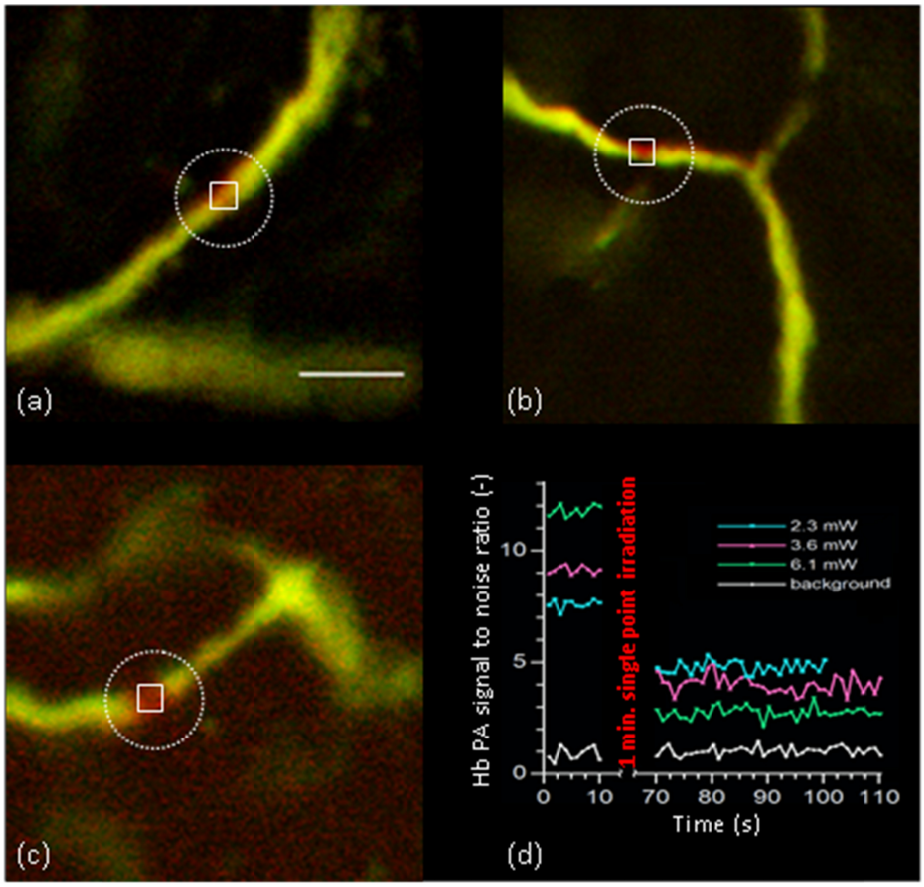

Fig. 5. Effect of single point laser irradiation (λ_{ex} = 415 nm) during 1 minute inside a vessel of the mouse ear at different laser powers. (a) 2.3 mW, (b) 3.6 mW and (c) 6.1 mW, which is the maximum diode laser power. PA images are composite images of the sumslices before (red) and after (green) single point laser irradiation. Scale bar in (a) = 50 µm. For region of interest covering the red signal, the instant decrease of the Hb PA signal to noise ratios in time are shown in (d). This decrease was related to the laser powers.

Biomedical Optics EXPRESS

3.3 Simultaneous PA microscopy and PDT of methylene blue for the monitoring of the acute effects on the RBC distribution in microvessels

The final *in vivo* application is a simultaneous photo-activation of MB and monitoring the effects on the RBC distribution. The dye MB is used as agent in preclinical and clinical photo-dynamic therapy studies [8,9]. Here, MB was intravenously infused, photo-activated with an optical power of 6.1 mW at 660 nm in the whole image during scanning and detected inside the mouse ear (micro)vessels. In Fig. 6, the MB dye caused blood coagulation in mainly arteries and arterioles immediately after infusion, see high intensity spots in 6b and cyan signals in 6f. Indeed, image 6c, which is the sum of slices after photo-activation, show an important decrease of the RBC concentration with regions of less Hb PA signals, see white arrows. In Fig. 6(d), the composite images of the sum slices before activation (red signals) and the sum of slices after photo-activation (green signals) clearly indicate vessels with a strongly reduced RBC concentration (red vessels), increase of RBC concentration (green vessels) or vessel areas with no change in the RBC concentration (yellow areas). The Hb PA signal to noise ratios changes are shown for the different ROIs in Fig. 6(e) and confirm the color codes of image 6d. Only the curve of the yellow ROI-2 in Fig. 6(d) is made orange in Fig. 6(e) for a better visibility. The overall normalized Hb and MB PA signals of all vessels after multiplying the whole times series with a binary mask (vessel = 1, background = 0) is shown in Fig. 6(h). The overall RBC flux reduction was immediate when the MB infusion started (blue arrow). Indeed, an orthogonal view of X in time (see Fig. 6(g) and horizontal yellow line in Fig. 6(f)) show at the time of MB infusion (cyan signal) that the MB PA signals are hardly mixed with red Hb PA signals, which should have become violet signals otherwise. In a control experiment (see Fig. 7), the laser diode at 660 nm was set to 4.2 mW at the presence of MB, which induced not the effects as described above. Thus, photo-activation of MB caused blood coagulation and not the infusion of MB only.

The simultaneous detection of the endogenous dye Hb and photo-activation of MB is important in photo-dynamic therapy for on-line activation and monitoring of PDT effects. This permits to stop PDT as soon as maximum effects are reached in order to spare normal adjacent tissues.

Biomedical Optics EXPRESS

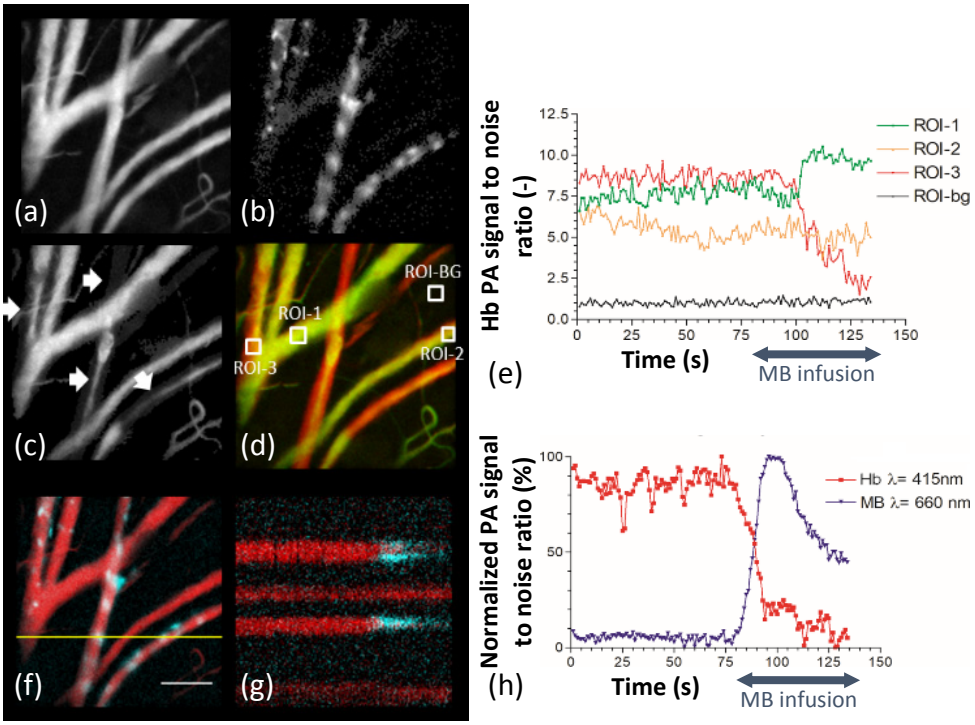

Fig. 6. PA-microscopic images (128 × 128 pixels) of vessels in a mouse ear after dual excitation and detection of hemoglobin and methylene blue (MB), scale bar in (f) = 50 µm. (a) The sum of the Hb PA signal intensities of all slices in time series of 133 images. (b) The sum of the last 40 images after the infusion of MB for the detection channel: λ_1 = 660 nm. Photo-activation of MB caused a denaturation of plasma proteins that formed blood clots and closed the vessels. (c) The sum of the last 40 Hb images after the infusion of MB (0.2 ml, 10 mg/ml, during 1 minute). Different vessels show a reduced or complete hemostasis, loss of hemoglobin signal, after photo-activation of MB, see white arrows. (d) Composite image of sum of Hb PA signal intensities before (= red, number of images = 53) and after MB photoactivation (= green, number of images = 53). Green stained vessel regions showed an increase of the RBC concentrations (see ROI-1), red vessel regions had a complete blocking of RBC flux (see ROI-3), yellow (see ROI-2) = no change, bg = background. (e) Plot of Hb PA signal to noise ratios changes in time for the ROI's in (d). (f) Sum of all slices in both channels: composite image, where Hb = red and MB = cyan. The yellow line defines the orthogonal view of X in time as shown in (g). (h) The normalized PA signal to noise changes in time for both channels for all vessels in all slices in time after background correction (rolling ball algorithm, radius = 20 pixel).

Biomedical Optics EXPRESS

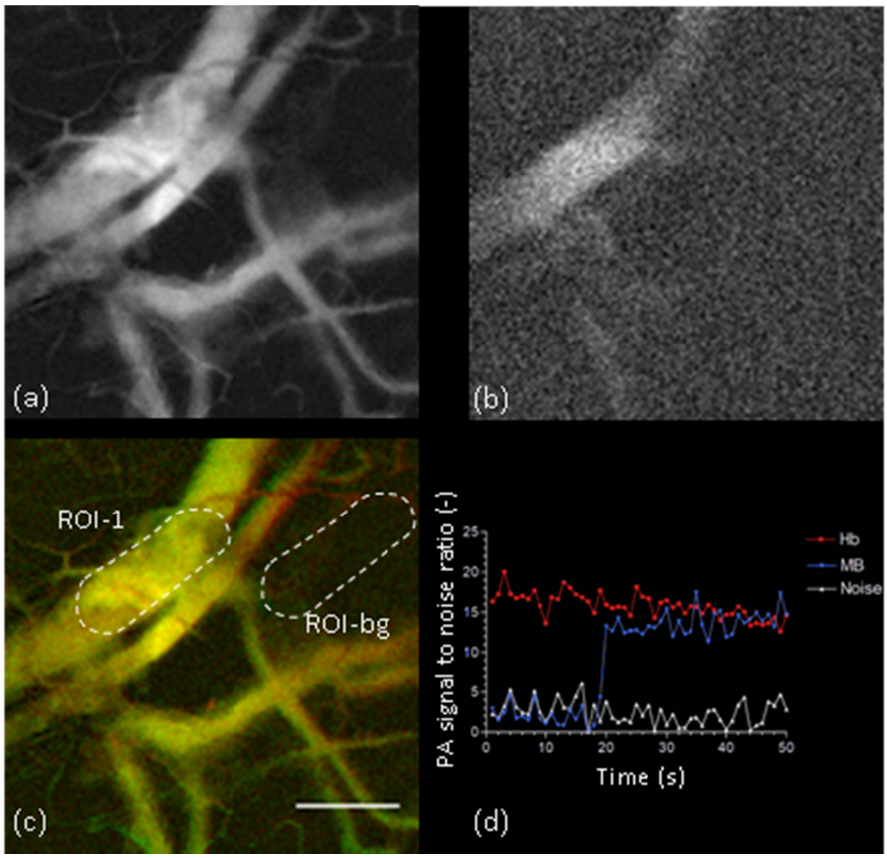

Fig. 7. Control of methylene blue infusion on the Hb distribution. The diode lasers at 415 nm and 660 nm were respectively set to 2.3 mW and 4.2 mW to avoid photo-activation of MB. The scale bar = 50 µm. (a) The sum of all 50 Hb PA images in the time series after background correction (rolling ball radius = 20). (b) The sum of the last 30 MB PA images after 1 minute MB infusion (0.2 ml, 10 mg/ml). (c) Composite image of 20 Hb PA images in red before MB infusion and 20 Hb PA images at the end of the times series in green after MB infusion showing most vessels in yellow (= red + green), which means no change in RBC distribution. (d) Graph of the normalized PA signal to noise ratios in time for the depicted vessel (ROI-1) and background noise level (ROI-bg) in (c) that confirms the yellow color code in (c).

4. Conclusion

We designed a photoacoustic microscope combining the beams of two laser diodes. By modulating the intensity of these laser diodes at different frequencies, two different dyes can be imaged simultaneously in the same sample. We have shown that at low laser power (2.3 mW), it is possible to image microvasculature *in vivo* without damaging tissue. These images can then be used for simultaneous photo-dynamic therapy at high laser power (> 6 mW) and monitoring of its effects on the RBC distribution. The generation of composite images, with a temporal color code, permit to analyze directly local changes in the RBC distribution or hematocrit after an intervention or changes in vessel reactivity (see Fig. 6(d)). The current configuration of the PA microscope with the piezo-electric transducer in the transmission mode can be easily converted in an epi-collection mode for the construction of a hand held device [3]. Finally, the techniques used for the realization of our microscope can be implemented with relatively inexpensive components in comparison with time domain photoacoustic systems or other imaging modalities.

Biomedical Optics EXPRESS

Funding

'La ligue contre le cancer, comité Isère'. We thank 'Centre National d'Etudes Spatiales' (CNES) for funding.

Disclosures

The authors declare that there are no conflicts of interest related to this article.

References

1. L. Hamard, D. Ratel, L. Selek, F. Berger, B. van der Sanden, and D. Wion, "The brain tissue response to surgical injury and its possible contribution to glioma recurrence," J. Neurooncol. **128**(1), 1–8 (2016).
2. M. Toi, Y. Asao, Y. Matsumoto, H. Sekiguchi, A. Yoshikawa, M. Takada, M. Kataoka, T. Endo, N. Kawaguchi-Sakita, M. Kawashima, E. Fakhrejahani, S. Kanao, I. Yamaga, Y. Nakayama, M. Tokiwa, M. Torii, T. Yagi, T. Sakurai, K. Togashi, and T. Shiina, "Visualization of tumor-related blood vessels in human breast by photoacoustic imaging system with a hemispherical detector array," Sci. Rep. **7**(1), 41970 (2017).
3. C. Canal, A. Laugustin, A. Kohl, and O. Rabot, "Portable multiwavelength laser diode source for handheld photoacoustic devices," Proc. SPIE **9887**, 98872B (2016).
4. P. Leboulluec, H. Liu, and B. Yuan, "A cost-efficient frequency-domain photoacoustic imaging system," Am. J. Phys. **81**(9), 712–717 (2013).
5. G. Langer, B. Buchegger, J. Jacak, T. A. Klar, and T. Berer, "Frequency domain photoacoustic and fluorescence microscopy," Biomed. Opt. Express **7**(7), 2692–2702 (2016).
6. C. Lange and P. J. Bednarski, "Photosensitizers for Photodynamic Therapy: Photochemistry in the Service of Oncology," Curr. Pharm. Des. **22**(46), 6956–6974 (2016).
7. S. Mordon, P. Deleporte, and N. Reyns, "A novel device for intraoperative photodynamic therapy dedicated to glioblastoma treatment," Future Oncol. **13**, 2441–2454 (2017).
8. A. F. Dos Santos, L. F. Terra, R. A. M. Wailemann, T. C. Oliveira, V. M. Gomes, M. F. Mineiro, F. C. Meotti, A. Bruni-Cardoso, M. S. Baptista, and L. Labriola, "Methylene blue photodynamic therapy induces selective and massive cell death in human breast cancer cells," BMC Cancer **17**(1), 194 (2017).
9. B. Kofler, A. Romani, C. Pritz, T. B. Steinbichler, V. H. Schartinger, H. Riechelmann, and J. Dudas, "Photodynamic Effect of Methylene Blue and Low Level Laser Radiation in Head and Neck Squamous Cell Carcinoma Cell Lines," Int. J. Mol. Sci. **19**(4), 1107 (2018).
10. M. S. C. Dos Santos, A. L. Gouvêa, L. D. de Moura, L. G. Paterno, P. E. N. de Souza, A. P. Bastos, E. A. M. Damasceno, F. H. Veiga-Souza, R. B. de Azevedo, and S. N. Báo, "Nanographene oxide-methylene blue as phototherapies platform for breast tumor ablation and metastasis prevention in a syngeneic orthotopic murine model," J. Nanobiotechnology **16**(1), 9 (2018).
11. L. Wang, K. Maslov, and L. V. Wang, "Single-cell label-free photoacoustic flowoxigraphy *in vivo*," Proc. Natl. Acad. Sci. U.S.A. **110**(15), 5759–5764 (2013).
12. L. Wang, K. Maslov, J. Yao, B. Rao, and L. V. Wang, "Fast voice-coil scanning optical-resolution photoacoustic microscopy," Opt. Lett. **36**(2), 139–141 (2011).